assuming that after $i-1$ transmissions the first negatively acknowledged codeword is in position $b_{i-1}+1$, is given by

$$q(b_i/b_{i-1}) = P_D(1-P_D)^{b_i-b_{i-1}} \tag{1}$$

where P_D is the probability of detecting in error a codeword belonging to code C. The probability $P_s(i)$ that after the ith transmission ($i \geq 1$) all the codewords of the jth group have been recovered can be expressed as

$$P_s(i) = \sum_{b_1=0}^{M-1} \sum_{b_2=b_1}^{M-1} \cdots \sum_{b_{i-1}=b_{i-2}}^{M-1} P_D(1-P_D)^{b_1} \times P_D(1-P_D)^{b_2-b_1} \cdots P_D(1-P_D)^{b_{i-1}-b_{i-2}}(1-P_D)^{M-b_{i-1}} \tag{2}$$

Therefore, it is

$$P_s(i) = \binom{M+i-2}{i-1} P_D^{i-1}(1-P_D)^M \tag{3}$$

We now evaluate the number n_j of time slots required to transmit the jth codeword group. During the ith transmission ($i \geq 1$) of the jth group, the number n_i of time slots in the ith transmission of the jth group is

$$n_i = N + b_i - b_{i-1} \tag{4}$$

If after i transmissions, the jth group is recovered (i.e. $b_i = M$), it can be easily shown that

$$n_i = i(N-1) + M \tag{5}$$

The mean number n_s of time slots required to transmit the jth group is

$$n_s = \sum_{i=1}^{\infty} n_i P_s(i) = \sum_{i=1}^{\infty} [i(N-1)+M]\binom{M+i-2}{i-1} P_D^{i-1}(1-P_D)^M \tag{6}$$

The throughput of the SW1 protocol is

$$T = \frac{kM}{n_s n} \tag{7}$$

In the following a code C of type (1023, 983) is considered.

The code C is assumed to be a perfect error-detecting code, i.e. one able to detect all error patterns. This hypothesis allows determination of a lower bound on the throughput. The communication channel has a bit error probability p; therefore, $P_D = 1-(1-p)^n$.

Fig. 2 shows the throughput T of the SW1 protocol against the channel error probability for different values of M for $N = 50$. The throughputs of the classical SW, GBN and SR schemes are also shown for comparison. The gains in throughput using SW1 with respect to the classical SW scheme are quite high for low and medium error probabilities p and with a suitable choice of M. It can be noted that, for mean and high error probabilities, the SW1 scheme presents throughput values near to those of the GBN protocol. However, the SW1 scheme requires a lower energy for information symbol than the GBN scheme.

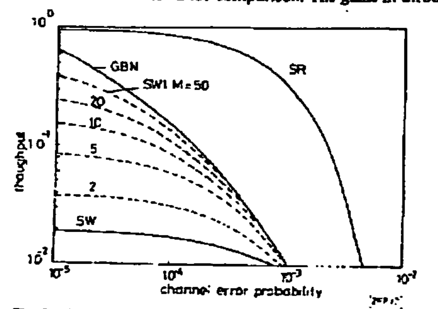

Fig. 2 *Throughput of SW1 protocol against channel error probability for $N = 50$*

3rd March 1992

F. Argenti and A. Garzelli (*Dipartimento di Ingegneria Elettronica, Università di Firenze, via S. Marta 3, 50139 Firenze, Italy*)

G. Benelli (*Dipartimento di Elettronica, Università di Pavia, via Abbiategrasso 209, 27100 Pavia, Italy*)

References

1 LIN, S., and COSTELLO, JR, D.: 'Error control coding: fundamentals and applications' (Prentice Hall, Englewood Cliffs, New Jersey, 1983)

2 LIN, S., COSTELLO, JR, D., and MILLER, M. J.: 'Automatic-repeat-request error-control schemes', *IEEE Commun.*, December 1984, 22, pp. 5–17

NOVEL FAST GPS/GLONASS CODE-ACQUISITION TECHNIQUE USING LOW UPDATE RATE FFT

A. J. R. M. Coenen and D. J. R. Van Nee

Indexing terms: Radiocommunication, Fourier transforms, Radionavigation

A novel 'differential' decoding technique is proposed which enables pre-averaging instead of postintegration for a substantially low update rate 'FFT-IFT' correlation in spread-spectrum (navigational) receivers. N-channel code acquisition can be performed to monitor the time dispersion with FFT time left to analyse frequency dispersion in highly reflective areas (e.g. an urban environment).

Introduction: Both frequently occurring line-of-sight (LOS) interruptions of NAVSTAR/GPS (the American military global positioning system) or GLONASS (the Russian GPS counterpart) signals and the multipath (MP) signals in the urban environment require a new generation of robust receivers (RXs). MP causes 'time dispersion' of the triangular correlation peak degrading the positioning accuracy. Moreover because of the relative movement between satellite and RX, both LOS and MP signals are affected by the Doppler effect. Especially when an RX is moving at a high speed (e.g. 70 km/h), the carrier Doppler spectrum may show 'frequency dispersion' up to 100 Hz causing false carrier locks and degrading data recovery. With respect to Reference 1, in this Letter an enhanced fast code-acquisition method is proposed to reduce the FFT (fast Fourier transform) and IFT (inverse FFT) update rate (= 1 ms per channel) substantially (> 100 times) to liberate enough FFT time to manage N channels and to calculate an extra N carrier Doppler spectra for frequency dispersion analysis to achieve (not shown here) enhanced data recovery for coherent RX operations by methods such as 'maximal ratio combining' or 'resolvable paths' [2]. The proposed method has led to a Dutch patent application [3] which covers the direct-sequence (DS) spread-spectrum (SS) communication area. It involves a grading in a fast, coarse to finer, code acquisition in a noncoherent way.

Differential decoding: In every single received DSSS LOS signal the code $c(t)$ in the baseband signal $bb(t)$ will be inverted permanently by its data signal $d(t)$ and by its (after down conversion) residual carrier signal $cc(t)$

$$bb(t) = cc(t)d(t)c(t) \tag{1}$$

where $ca(t) = A \cos(2\pi f_{rc} t + \phi)$. By selecting the residual by Doppler $(-5\,\text{kHz} < f_{caD_0} < 5\,\text{kHz})$ modulated carrier frequency f_{rc} (e.g. ~ 0 Hz), the carrier evoked inversion rate can be kept relatively low. Compared with the chip rate $f_c = 1/T_c = 1{\cdot}023$ Mchip/s (GPS) or 511 kchip/s (GLONASS) the data inversion rate ($f_d = 1/T_d = 50$ bit/s) is already significantly low. Then, almost all the transition positions in $bb(t)$ are due to code (or chip) edges. The novel proposed correlation technique is based on chip-edge correlation (or matching) regardless of the sign of the edge. Similarly the DPSK (differential phase-shift keying) demodulation [4] can be performed by a 'T_c delay and multiply' operation (i.e. $bb(t) \cdot bb(t - T_c)$). To perform correlation the local generated replica code c_{ref} has to undergo the same differential decoding (DD), i.e. $c_{ref}(t) \cdot c_{ref}(t - T_c)$. However, in practice the SS RX baseband signal-to-noise ratio (SNR) is below zero (GPS, GLONASS: $SNR < -15$ dB). As a penalty for the gained Doppler and data insensitivity, a single differential stage causes a squared increase of the baseband noise power ($SNR < -30$ dB). A partial regain of lost SNR arises by extending this method to M different stages of 'm times T_c delay and mulitply' and summing the correlation functions for each M

$$\Delta(SNR_M)_{max} = 10 \log M \qquad \text{(dB)} \quad (2)$$

Theoretically, if f_{rc} is adjusted to 0 Hz, eqn. 2 is valid for every M value with $M_{max} = 1023$ (GPS) or 511 (GLONASS). However, as a practical value, $M < 32$ (i.e. $m = \{1, \ldots, 32\}$) should be chosen if $(f_{rc})_{max} < 20$ kHz; then, $32T_c \ll (1/4)(1/f_{rc})$ should be obeyed for an effective DD operation. In that case, every received satellite signal can be processed simultaneously providing the correlator input signal for coarse acquisition.

Pre-averaging by comb filtering: As a second and more profitable recovery method, using the code sequence periodicity $T_p = 1023T_c$ (GPS) or $511T_c$ (GLONASS), a simple integrate and dump (I&D) type comb filter with a feedback delay of T_p to perform an averaging operation enables at least a recovery of the original baseband SNR or even more.

$$\Delta(SNR_{av})_{max} = 10 \log b \qquad \text{(dB)} \quad (3)$$

where $b = T_{av}/T_p$ and T_{av} is the averaging time. To avoid time dispersion (caused by a code Doppler f_{coD_0} of a few Hertz) of say xT_c $(x < 1)$ by averaging, $f_{rc} = f + nf_c/2$ with $n = \{0, 1, 2, \ldots\}$ should be chosen accordingly:

$$f < rx/T_{av} \quad (4)$$

Here r represents the ratio between the received carrier and chip frequency ($r = f_{caD_0}/f_{coD_0}$) with $r = 1540$ (GPS), $r \simeq 3000$ (GLONASS). Example: $T_{av} = 0{\cdot}1$ s, $x = 0{\cdot}01$ and $r = 1540$ then $f < 154$ Hz, while eqn. 3 shows a $+20$ dB regain. By averaging, combined with M extended DDs, the recovered SNR according to eqns. 2 and 3 is just enough ($SNR > -13$ dB) to obtain correlation with a detection probability of 0·99 [1]. Here, the process gain by an FFT correlation over 1023 chips amounted to ($10 \log 1023 \simeq$) 30 dB. With respect to Reference 1, choosing $T_{av} > 0{\cdot}1$ s, the FFT update rate can be reduced by more than ($b =$) 100.

Extended differential decoder (EDD): Without efficient use of pseudorandom noise (PRN) properties such as 'cycle and add' (C&A), parameter M and the hardware complexity have a proportional relation. Applying the C&A property coherent to the DD operations on GPS Gold codes G_i ($i = \{1, 2, \ldots, 1023\}$), it can be proven that one G_i changes into two identical Gold-codes (i.e. $m = \{341, 682\}$) plus four groups of 255 other unique Gold codes G_{im} within the class of G_i with 1022 unique code offsets CO_{im} ($m = \{1, 2, \ldots, 1022\}$). For GLONASS, only the code offset of the single linear maximum length sequence (LMLS) of 511 chips will be affected by DD, not the LMLS itself. A proposed structure is shown in Fig. 1 for a GPS system. In Fig. 1 the tapped delay line (TDL) compensates for code offsets for each m value which allows the same code to be originated. Each tap distance per differential stage equals an $m \cdot T_c$ delay. For GPS there are unfortunately only groups of four m values resulting in the same code (e.g. $m = \{8, 25, (1023\text{-}8), 1023\text{-}25\}$), but luckily for GLONASS there is no limitation (e.g. $m = \{1, 2, \ldots, 32\}$). The digitised $bb(t)$ as TDL input signal can be an oversampled two-level signal for ease of multiplication by EXORs. A bit-count operation is followed by an I&D filter as decimator (to $2f_c$ Hz), which forms the input signal to an averager. After T_{av} s the averager register is

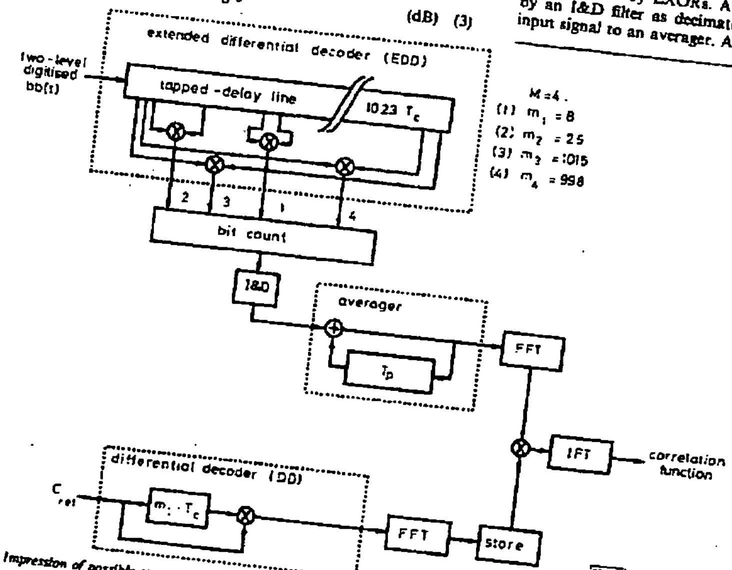

Fig. 1 *Impression of possible structure with EDD/averager combination for GPS*
For example $m = \{8, 25, 998, 1015\}$ leads to same Gold code
EDD for GLONASS can be made much more efficient by its LMLS code property

read out (dumped) to perform correlation (by multiplication in the frequency domain) with c_{ref}. A further increase of M for GPS arises by additionally selecting other groups of four m values. The results should be correlated separately by spectral multiplication, then the product spectra per group are added and finally only one IFFT for the final correlation function generation is applied. According to a strict scheme (not shown here) the TDL in Fig. 1 can be adapted easily for GLONASS for $M = 32$ and $m = (1, 2, \ldots, 32)$. In a cold start situation we may start with $T_m = 0{\cdot}1$ s, low m values and $|f_{rc}| < 5$ kHz to find correlation with each of the satellite constellation expected c_{ref} signals coarsely, using only one EDD/averager combination. After a better carrier estimation according to eqn. 4 with one combination per c_{ref}, the code acquisition will be far more precise. Especially in a rate-aided tracking situation T_m may increase dramatically.

Conclusions: Differential decoding combined with comb-filter averaging makes the exploitation of the FFT highly efficient for N-channel correlation operations and for frequency-dispersion monitoring. Coarse code acquisition can be performed within the whole Doppler range for a < 1 s cold start. Fine control arises by a more precise carrier estimation especially in rate-aided tracking.

Acknowledgment: The authors would like to thank C. M. van der Knaap for his numerous model verifications by computer simulations, A. Jansveld for his work on code analysis, and D. van Willigen and R. Prasad for their useful comments.

30th January 1992

A. J. R. M. Coenen and D. J. R. Van Nee (*Telecommunications and Traffic-control Systems Group, Delft University of Technology, PO Box 5031, 2600 GA Delft, The Netherlands*)

References

1 VAN NEE, D. J. R., and COENEN, A. J. R. M.: 'New fast GPS code-acquisition technique using FFT', *Electron. Lett.*, 1991, 27, (2), pp. 158–160
2 PROAKIS, J. G.: 'Digital communications' (McGraw-Hill, New York, 1989), 2nd edn.
3 COENEN, A. J. R. M.: 'Method and appliance for fast code-acquisition in spread spectrum receivers'. Dutch patent application, 2 July 1991, No. 0.A. 91.01155 Ned.
4 CARLSON, A. B.: 'Communication systems' (McGraw-Hill Book Co., Singapore, 1986), 3rd edn. (student), pp. 539–541

EXTENDED TRENCH-GATE POWER UMOSFET STRUCTURE WITH ULTRALOW SPECIFIC ON-RESISTANCE

T. Syau, P. Venkatraman and B. J. Baliga

Indexing terms: Field-effect transistors, Transistors, Semiconductor devices and materials

An ultralow specific on-resistance power UMOSFET structure with the trench-gate extending down to the N^+ substrate is presented. Specific on-resistances in the range 100–200 $\mu\Omega\,cm^2$ have been experimentally demonstrated for devices capable of supporting up to 25 V. Comparison of theoretical and experimental results is provided.

Introduction: Power MOSFETs with breakdown voltages in the 10–50 V range, operated as synchronous rectifiers, have been suggested to replace Schottky diodes in the output stage of power supplies for output voltages below 5 V [1]. For these power MOSFETs to be used as low-voltage rectifiers, however, the power loss in the forward conduction state must be as low as possible, i.e. a further reduction in the device specific on-resistance is demanded. The UMOSFET structure [2–4] is believed to be a good solution for obtaining low specific on-resistance. For 30 V devices, a specific on-resistance of 1000 $\mu\Omega\,cm^2$ has been reported by Chang *et al.* [4]. In comparison, 50 V devices have been reported most recently by Matsumoto *et al.* [5] with $R_{on,sp} = 580\,\mu\Omega\,cm^2$.

This Letter describes a new power MOSFET structure, called the modified mode field-effect transistor (MMFET), having an ultralow on-resistance approaching 100 $\mu\Omega\,cm^2$ for a device with a breakdown voltage of 25 V. This improved performance results not only from the inherent features of the UMOSFET structure in eradicating the JFET pinching effect and increasing the channel density, but a unique feature of the MMFET where the current flows from the base to the drain via a highly conductive accumulation layer rather than by spreading into a drift region as in previous UMOSFET structures.

Device structure: The vertical cross-sections of the proposed device (MMFET) and the conventional UMOSFET are shown in Fig. 1. The principal difference between these structures is that in the MMFET, the gate extends into the N^+ substrate. Consequently, the on-state current flows primarily along an accumulation layer formed on the trench sidewall, and, unlike the conventional UMOSFET, the drift region resistance does not contribute to the on-resistance in the MMFET. As a result, the doping concentration can be as low as possible for the drift region with a typical value of $10^{14}\,cm^{-3}$. With such low drift region doping, the maximum sustainable drain voltage for the MMFET device is determined by the punch-through breakdown voltage of the P-base/N^-/N^+ structure as long as the oxide in the gate-drain overlapping region is sufficiently thick to support the voltage. For the conventional UMOSFET, however, an optimum

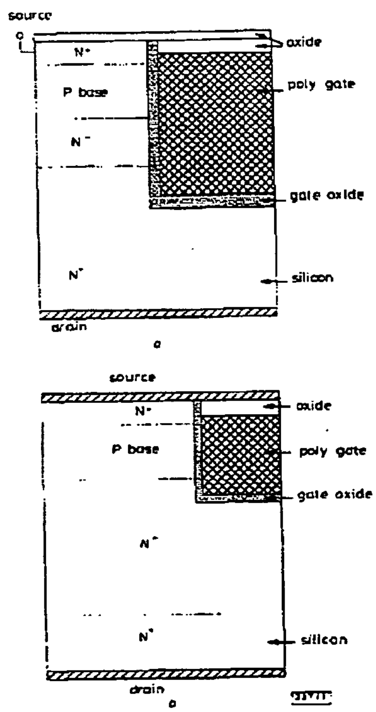

Fig. 1 *Cross-section views of new MMFET structure and conventional UMOSFET structure*
a MMFET
b UMOSFET

BEST AVAILABLE COPY

1

length ratios of u/L, v/L and w/L are 0·3, 0·4, and 0·3, respectively. As indicated in Fig. 2, more than −20dB crosstalk level of bar state can be expected over the range from 3 to 4 of $\Delta\beta_{TM}/\Delta\beta_{TE}$. By designing the length of each section (u, v, w) adequately, a voltage controlled optical power splitter can be produced as shown in Fig. 3. Uniform $\Delta\beta$ elements, whose L/l_{TM} and L/l_{TE} were about 1 and 3, were used to measure the ratio a. The measured ratio a was from 3·6 to 3·8 in our experiment and was bigger than the previously reported values.[3,5] This is presumably due to the difference in mode confinement conditions for TM and TE modes between measured directional couplers. However, a of around 3·7 is favourable for the performance of the device proposed.

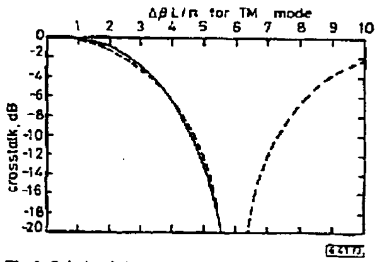

Fig. 3 *Calculated characteristics as optical power splitter*
$u/L = 0{\cdot}3675$; $v/L = 0{\cdot}265$; $w/L = 0{\cdot}3675$; $a = 3{\cdot}6$

Fabrication: The coupling length conditions for the TM and TE modes were satisfied when 750Å-thick titanium, 7 μm width, and 7 μm spacing patterns were diffused at 1050°C for 6h in a wet Ar atmosphere. The length of each section was determined based on the measured $\Delta\beta_{TM}/\Delta\beta_{TE}$. The coupling effects of the curved guide regions (R = 40mm) at the both sides of directional couplers for the TM and TE modes were also considered to define electrode photomask patterns. These coupling effects were measured by comparing the output light intensities from the guides of directional couplers with theoretical values, and their estimated values in terms of coupling length were less than 1 mm for both modes. From these fundamental data, devices with the length ratios of $u/L = 0{\cdot}375$, $v/L = 0{\cdot}25$, and $w/L = 0{\cdot}375$ (L = 22mm) were fabricated for optical power splitters.

Experimental results: The device characteristics were measured by PMF endfire coupling at 1·31 μm wavelength. A computer controlled measurement system with a IR camera and a voltage generator was used. Digital video signals from the IR camera were integrated and computed to measure crosstalk values.

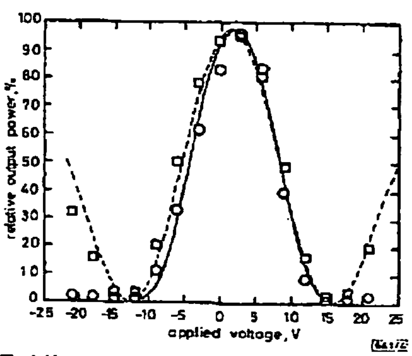

Fig. 4 *Measured and calculated characteristics*
○ measured for TM mode
□ measured for TE mode
——— TM mode
- - - - TE mode
$u/L = 0{\cdot}375$; $v/L = 0{\cdot}25$; $w/L = 0{\cdot}375$; $a = 3{\cdot}5$; $L = 22$mm

Fig. 4 shows the measured optical output intensities for both polarisations as functions of the applied voltages. In the Figure, calculations are also plotted. The ratios of the coupling length to the complete coupling lengths were about 0·9 for the TM mode and about 2·9 for the TE mode. As predicted by the calculations, the switching voltages for the TM and TE modes are coincident, and the applied voltage dependence of the output light intensities for the TM mode is also coincident with that for the TE mode. The switching voltage is relatively low, about 15 V.

Conclusion: New polarisation-insensitive devices, based on the modified configuration of three section alternating $\Delta\beta$, have been produced in Z-cut $LiNbO_3$. Polarisation-insensitive switching and power splitting characteristics have been obtained.

N. KUZUTA
K. TAKAKURA

Shimadzu Co. Opto-electronics Department
2385-13 Ihiyama Atsugi, Kanagawa 243-02, Japan

26th November 1990

References

1 OKAYAMA, H., MATOBA, A., SHIBUYA, R., and ISHIDA, T.: 'Polarisation independent optical switch with cascaded optical switch matrices', *Electron. Lett.*, 1988, 24, pp. 959–960
2 GRANESTRAND, P., LAGERSTRÖM, B., SVENSSON, P., THYLEN, L., STOLTZ, B., BERGVALL, K., and OLOFSSON, H.: 'Tree-structured polarisation independent 4 × 4 switch matrix in $LiNbO_3$', *Electron. Lett.*, 1988, 24, pp. 1198–1200
3 KONDO, M., OHTA, Y., TANISAWA, Y., AOYAMA, T., and ISHIKAWA, R.: 'Low-drive-voltage and low-loss polarisation independent $LiNbO_3$ optical waveguide switches', *Electron. Lett.*, 1987, 23, pp. 1167–1169
4 KOGELNIK, H., and SCHMIDT, R. V.: 'Switched directional coupler with alternating $\Delta\beta$', *IEEE J. Quantum Electron.*, 1976, QE-12, pp. 396–401
5 HABARA, K.: '$LiNbO_3$ directional coupler polarisation splitter', *Electron. Lett.*, 1987, 23, pp. 614–616

NEW FAST GPS CODE-ACQUISITION TECHNIQUE USING FFT

Indexing terms: Correlation, Fast Fourier transforms

A new spread-spectrum code-acquisition technique for the navigation systems Navstar/GPS and Glonass is introduced. This technique uses the FFT to compute the correlation function, thereby eliminating the time-consuming code phase shift process. Comparisons with existing systems show a theoretical reduction in acquisition time of about 2000 times.

Introduction: A short acquisition time is very important for a standard positioning service Navstar/GPS or Glonass receiver, especially in an urban environment where satellites are often visible for a few seconds only. In this case, an acquisition time of less than a few seconds is desired to avoid the receiver having to continuously remain in the acquisition phase. We discuss the code acquisition time only, that is, the time needed to align the incoming code and the local code within one chip. The proposed new acquisition technique is a result of our research into satellite navigation in an urban environment.

Noncoherent correlator: The most frequently used code acquisition system is the noncoherent correlator, shown in Fig. 1.[1,2] The incoming signal $x(t)$ consists of noise plus the GPS signals which have a carrier frequency of 1·6GHz, and are binary phase modulated by a Gold sequence of 1023 chips with a chip rate of 1 MHz, and by a 50 Hz data stream. This signal is converted to baseband and coherently correlated with the local code for NLT_c seconds. Here L is the code length

(= 1023 chips for the C/A code), T_c is the chip time and N is an integer ≥ 1. This time is chosen short enough to ensure that the presence of data and carrier Doppler shift will not cause a great degradation in performance.[3] Next, K sequential correlations are noncoherently summed to produce one correlation point at a sufficiently high signal-to-noise ratio. The total integration time $KNLT_c$ is called the dwell time.

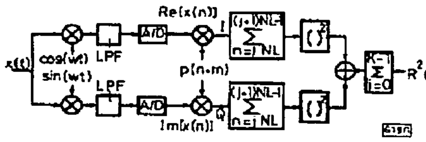

Fig. 1 *Noncoherent correlator in time domain*

To achieve acquisition with the noncoherent correlator, the above procedure has to be performed for all possible code phases and also for a number of possible Doppler frequencies, because the carrier phase has to remain nearly constant during individual integration times NLT_c. As a result, the acquisition time is proportional to the number of cells, which is defined as the product of the number of code phase steps and the number of carrier frequency steps. For GPS, a typical value of the number of cells is 20460 for half a chip phase step (2046 steps for the C/A code) and 1 kHz carrier frequency step at a correlation time of 1 ms ($N = 1$) and a carrier Doppler range of 10 kHz, neglecting the contribution due to the speed of the receiver.

Parallel search techniques using the FFT: To reduce the acquisition time, cells can be searched in parallel by taking the FFT of the complex samples at the points I and Q in Fig. 1.[3] At the moment that the incoming code and the local code have the same phase, a carrier component will be present in the spectrum, which is visualised by the FFT. Using this technique only 2046 phase steps remain, reducing the acquisition time ten times in comparison with the first system, assuming the FFT can be computed within the dwell time.

In the above system, a parallel search in frequency is performed to eliminate 10 frequency search steps. In our proposed system, a parallel search in time is performed, i.e. all points of the correlation function are calculated from the same input sequence, with a theoretical gain in acquisition time of 2046 times in comparison with the conventional correlator, which is much more than the gain of the previous system that also uses a digital signal processor, but in a completely different way.

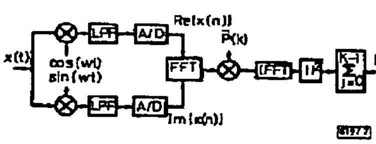

Fig. 2 *Noncoherent correlator via frequency domain*

The correlation operations are implemented as follows (see Fig. 2). A digital signal processor loads $2NL$ complex samples with a time spacing of half a chip and then performs the correlation operation

$$R(m) = \sum_{n=0}^{NL-1} x(n) \cdot p(n+m) \qquad \text{for } m = 0, 1, \ldots, 2L-1 \quad (1)$$

The processor stores all $2NL$ points of $R^2(m)$ in an accumulator. This process is repeated until K separate correlation functions have been summed.

Unfortunately, a straightforward calculation of $R(m)$ requires a large number of operations, which is proportional to $(NL)^2$. Much computing time can be saved, however, if the correlation function is calculated via the frequency domain:[4]

$$R(m) = x(n) * p(-n) = F^{-1}[X(k) \cdot \bar{P}(k)] \quad (2)$$

where $*$ represents convolution, $X(k)$ is the spectrum of $x(n)$, $\bar{P}(k)$ is the complex conjugate of the spectrum of $p(n+m)$ and F^{-1} is the inverse Fourier transform.

The fastest FFT algorithms require the number of points to be radix 2. We therefore add two zeros in both incoming and local code with a spacing of half the code length. In fact, we slightly deform the codes, which yields the advantage of fast processing but has the disadvantage of a somewhat larger crosscorrelation. The latter effect, however, is negligible compared to the thermal noise level in the acquisition phase.

Because the digital signal processor computes the entire correlation function in one dwell time, this technique is theoretically 2046 ($2L$) times faster than the previously mentioned parallel frequency search method, which uses the same amount of hardware. In practice, this gain will only be achieved if the signal processor is fast enough to compute $2K$ times a $2NL$ point FFT within one dwell time. Also, this has to be done for at least ten different carrier frequency steps; for each frequency step the input signal is frequency shifted through a software-implemented image-rejection mixer. For the typical values $K = 20$, $N = 1$ and ten frequency steps, this would mean that ten 2048 point FFTs have to be computed within 500 µs. Such signal processors actually exist but are still extremely expensive. However, even with the TMS320C30 processor we use, an estimated minimum acquisition time of less than 500 ms per frequency step is possible, which then yields a gain in acquisition time of eight times compared to the parallel frequency search system. In the case of reacquisition, which will occur frequently in an urban environment, the carrier frequency will often be known accurately enough to reduce the number of frequency search steps to only one, so the gain in acquisition time of the TMS320C30 can be increased by a factor ten.

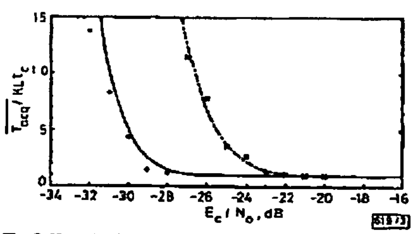

Fig. 3 *Normalised mean acquisition time as function of the signal-to-noise ratio for K = 20 and K = 4*

——— $K = 20$
— · — $K = 4$
+ simulated results for $K = 20$
× simulated results for $K = 4$
$L = 1023$ $c = 5$

Finally, to demonstrate that the system actually works, Fig. 3 shows a plot of the mean acquisition time as a function of the signal-to-noise ratio E_c/N_0 which is calculated using the equations described in Reference 3. For a number of different signal-to-noise ratios, we simulated a GPS spread-spectrum signal with additive Gaussian noise. We performed 100 simulations for each value of the signal-to-noise ratio, and counted the number of successful acquisitions, which is a measure of the acquisition probability p that can be substituted in the equation for the mean acquisition time in the case of a single dwell acquisition procedure (for $N = 1$)

$$\frac{\overline{T_{acq}}}{KLT_c} = \sum_{i=0}^{\infty} [ic + (i+1)] \cdot (1-p)^i \cdot p = \frac{1 + c \cdot (1-p)}{p} \quad (3)$$

The constant $c \cdot KLT_c$ is the penalty time in the case of a false alarm. As can be seen, the simulated plots have a close resemblance to the calculated curves. The shift of about half a dB for $K = 20$ is most probably due to the approximations in the calculation, so we can conclude that the performance of the systems in Fig. 1 and 2 are the same, except for a constant factor in the acquisition time. It should be noticed that the mean acquisition time in Fig. 3 is multiplied by a certain

factor if the signal processor used is not processing in real time.

Conclusions: By using a digital signal processor in a hitherto unusual way, the code acquisition time of a GPS receiver can be reduced considerably. The fastest performance is achieved when the incoming code and the local code are slightly deformed by adding zeros, allowing the use of the FFT.

Acknowledgment: The authors would like to thank Mr. E. Theunissen and Mr. T. Lamerigts for their work on the TMS320C30 processor and Prof. D. van Willigen and Prof. R. Prasad for their helpful comments.

D. J. R. VAN NEE
A. J. R. M. COENEN

23rd November 1990

Telecommunications and Traffic-control Systems Group
Delft University of Technology
PO Box 5031, 2600 GA Delft, The Netherlands

References

1 HOLMES, J. K.: 'Coherent spread spectrum systems' (Wiley, New York, 1982), p. 423
2 CHERUBINO, G., and PUPOLIN, S.: 'Performance analysis of an all digital acquisition circuit', *IEEE Trans. Commun.*, 1985, 33, pp. 863–868
3 CHENG, U., HURD, W. J., and STATMAN, J. L.: 'Spread spectrum code acquisition in the presence of Doppler shift and data modulation', *IEEE Trans. Commun.*, 1990, 38, pp. 241–250
4 OPPENHEIM, A. V., and SCHAFER, R. W.: 'Digital signal processing' (Prentice-Hall, New Jersey, 1975), p. 556

INJECTION-LOCKING OF Q-SWITCHED AlGaAs LASER WITH FAST SATURABLE ABSORBER

Indexing terms: Semiconductor lasers, Lasers

Injection of a weak CW laser beam in a Q-switched AlGaAs laser diode with a fast saturable absorber is shown to produce powerful single-mode picosecond pulses at 0·82 μm. The saturable absorber regions are obtained by deep implantation of heavy ions through the diode facets. Single-mode operation is achieved with CW injection powers as low as 50 μW. Peak powers exceeding 1·5 W are detected at the laser output. A time-resolved spectroscopy of the laser pulses reveals an overall downchirp of 1·5 nm.

Introduction: Q-switching of (Al)GaAs laser diodes is now recognised as being a very efficient and simple technique to produce picosecond pulses in the 0·8–0·85 μm region.[1–3] Recently, 5 ps pulses with peak powers up to 5 W have been observed by using fast saturable absorbers.[4,5] Pulses produced by this technique, however, generally exhibit poor spectral characteristics that are not desirable for a number of applications. We demonstrate the possibility of controlling the laser spectrum with the injection of a weak CW beam into the cavity. Owing to the use of a very fast saturable absorber, output powers are ten times higher than those reported in the previous works on injection-locking of pulsed semiconductor lasers.[6] Moreover, time-resolved spectroscopy of the single-mode laser pulses reveals a downchirp of very large amplitude, which enables us to predict the feasibility of bandwidth-limited subpicosecond pulses.

Experimental setup: The experimental setup is shown in Fig. 1. The semiconductor laser is a GaAs/AlGaAs gain-guided double-heterostructure already described in previous works.[3–5] The active region is 200 μm long. The emission wavelength is in the 820–830 nm range. Internal Q-switching is obtained by producing regions of a saturable absorber near the mirrors of the laser resonator by 18 MeV implantation of nitrogen ions. With electrical pump pulses of 40 V amplitude, 1·5 ns risetime and 100 kHz repetition rate, the laser emits multimode optical pulses of 5–10 ps full width at half maximum (FWHM). The energy per facet is 15 pJ.

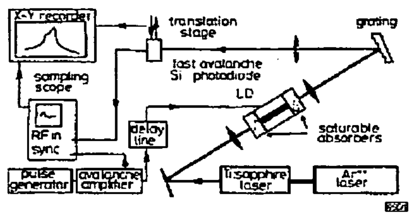

Fig. 1 *Experimental setup*

The laser mode control is presently achieved by injecting a weak CW tunable Ti : sapphire laser beam through one facet of the laser diode. A 0·1-NA $f = 20$ mm lens is used to focus the injection beam in the resonator. The CW infrared power incident onto the sample typically ranges from 10 to 100 μW, only 10% of which is estimated to be injected into the transverse resonator mode. The residual amount of power transmitted from the opposite facet of the laser diode is still one order of magnitude lower and typically represents less than 10% of the *average* output power delivered by the diode.

For spectral measurements, the output beam is diffracted with a 1200 g/mm grating after being collimated with a 0·35-NA $f = 10$ mm microscope objective. An $f = 50$ cm lens is then used to focus the diffracted beam either onto an infrared camera or a fast Si avalanche photodiode. The camera is used for rapid control of the laser spectrum. Injection-locking is seen to occur when one of the laser spots becomes much brighter than the others. For a more precise analysis, the camera is replaced by the fast photodiode, the latter having a detecting aperture of 50 μm. A spectral resolution of about 1 Å is obtained when scanning the photodetector across the beam.

The same arrangement is used to qualitatively analyse the wavelength evolution during the pulse. As shown in Fig. 1, the photodetector signal is fed into the 7S12 sampling unit of a Tektronix 7854 oscilloscope equipped with the S4 sampling head. Using the manual mode of operation, the signal is analysed in a temporal window of ~20 ps, the position of which can be adjusted with a precision of a few picoseconds with respect to the triggering pulse. The 7S12 unit output is then recorded while slowly scanning the photodetector across the diffracted beam. The operation is repeated for different positions of the temporal window. Because of the longer 100 ps response time of the photodetector as compared to the ~10 ps width (FWHM) of the optical pulses, the photodetector actually acts as an integrator. In other words, the procedure described above allows us to measure the time-averaged spectrum of the laser pulse for various averaging times in the tens of picoseconds scale. Although the resolution is limited by the width of the temporal window, we are able to determine the sign and the total amplitude of the wavelength shift during the pulse.

Experimental results: The efficiency of the injection-locking process is illustrated in Fig. 2. The bottom curve represents the multimode spectrum of the laser without injection. The pulse energy spreads over a dozen of the longitudinal modes, which approximately corresponds to a spectral width of 5 nm. The asymmetrical shape of the spectrum envelope indicates the presence of chirping effects. The top curve in Fig. 2 represents the laser spectrum under injection-locking conditions. Most of the pulse energy is now concentrated within a narrow spectral region located on the long wavelength side of the injection. The width of the spectral region essentially depends on the electrical pumping and typically ranges from 1·2 to 1·6 nm. The fraction of pulse energy contained within this region depends on the injection parameters. It increases with the injection power. At a given injection power, an optimum value is found when the injection is tuned near the gain maximum of the laser diode. For the case of Fig. 2, the injection power is 50 μW, the injection laser is tuned at 822 nm and